Science Forum (Journal of Pure and Applied Sciences)

Journal Homepage: https://atbuscienceforum.com.ng/index.php/jpas

Integrated Airborne Magnetic and Radiometric Data Analysis for the Delineation of Gold Mineralization Zones in North Central Nigeria

Abubakar Aliyu[1*], Aminu L. Ahmed[2], Muhammad B. B. Dewu[3], Seyi A. Sonloye[1], Abubakar Fahad[4], Joseph Omeiza Alao[5]

[1]Department of Physics University of Maiduguri
[2]Department of Physics, Ahmadu Bello University, Zaria
[3]Center for Energy Research and Training, Ahmadu Bello University, Zaria.
[4]Department of Geosciences, Confluence University of Science and Technology, Osara, Nigeria
[5]Department of Physics, Air Force Institute of Technology, Kaduna, Nigeria

Abstract

Recent advancements in geophysical methods and data processing techniques have renewed interest in the exploration of gold and associated mineral deposits, enhancing the effectiveness of these methods in identifying new mineralized zones. This study aims to delineate hydrothermal alteration zones linked to gold mineralization in a segment of North Central Nigeria using airborne geophysical datasets—specifically magnetic and radiometric data. A suite of signal enhancement techniques was applied, including vertical derivatives, analytic signal, CET grid and porphyry analysis, apparent susceptibility mapping, Euler depth deconvolution, potassium-thorium ratios, and ternary imaging. Magnetic data interpretation revealed a dominant NE–SW lineament trend, with secondary trends observed in the NW–SE, N–S, W–E, and NNE–SSW directions. High magnetic susceptibility values (0.0003–0.0007 SI) associated with the NE–SW trend suggest a structural control on mineralization and highlight prospective zones. Euler deconvolution indicated the depth of magnetic sources ranges from near-surface to approximately 1800 meters, corresponding to both shallow and deep-seated geological structures. Radiometric data further identified lithological units and hydrothermal alterations, with volcanic intrusions and structural lineaments spatially correlating with potential mineralized zones. Through integrated interpretation of these datasets, twelve new target areas with potential for gold mineralization have been delineated, providing valuable insights for future exploration efforts in the region.

Keywords
Gold, Exploration, Hydrothermal, Alteration, Structures, Potential, Apparent Susceptibility

Corresponding Author: Abubakar Aliyu, Department of Physics, University of Maiduguri Email: aliyu@unimaid.edu.ng

INTRODUCTION

The mapping of alteration zones has become of utmost importance due to their possible connection with commercially valuable mineral resources such as gold, nickel, arsenic, cobalt, wolframite, and mercury (Elkhateeb & Abdellatif, 2018; Mahdi et al., 2022). The most successful geophysical methods that can map alteration zones are magnetic and radiometric because of their definite definition of the subsurface geology in terms of lithology, hydrothermal, and structures like fault, shear zones, fractures, folds, contact, and veins that could serve as a conduit for ore deposit in the basement rocks (Aliyu et al., 2020b; Elkhateeb & Abdellatif, 2018).

The fundamental principle of aeromagnetic methods is the measurement of the ambient magnetic susceptibility of the surface geology, followed by the analysis of the data to determine the distribution of magnetic minerals and consequently changes in lithology (Telford et al., 2004). It can reveal contrasting patterns that may reflect differences in lithologic composition, lineaments, faults, contacts, crustal structures, and/or type and degree of alteration. Aeromagnetic methods are used in mineral exploration to identify features such as faults, folds, contacts, shear zones, and intrusions as well as to automatically find porphyry and promising ore deposit locations. (Eldosouky et al., 2020; Elkhateeb & Abdellatif, 2018).

The radiometric method on the other hand is a measure of the natural radiation in the earth's surface called gamma rays, which can tell us about the distribution of certain soils and rocks. It is frequently used as a geological mapping tool (Aliyu et al., 2020a; Boadi et al., 2013). This technique involves detecting naturally occurring radioactive elements in soil profiles and rock-forming minerals. These elements are uranium (U), thorium (Th), and potassium (K), which can be found as trace elements in all rocks and decay naturally to produce gamma radiation (gamma rays) (Boadi et al., 2013 and Ahmed 2018).

Several literatures have revealed many areas of gold occurrence in the Nigerian Schist Belts (Woakes., 1987; Akande, 1991, Garba and Akande, 1992; Garba, 2000 and 2002). Such areas include Minna-Birnin Gwari, Yauri-Anka-Maru in the northwest and Ife-Ilesha (Iperindo) Egbe-Isanlu-Dogondaji (Okolom) in the southwest. The investigated area is an extension of Ife-Ilesha of southwestern Nigeria (Aliyu et al., 2020b; Umaru et al., 2022).

Some researchers carried out studies in the investigated area including (Aliyu et al., 2020b) who delineated minor and major subsurface geological structures significantly trending NE-SW believed to have caused the mineralization of pegmatite. Udensi et al., (2003) analysed the magnetic field and revealed the presence of lineaments. Adeleye, (1973) carried out geological research and revealed rock contents of two distinct geological units as Basement Complex rocks including granites, biotite gneiss, amphibolite, pegmatite, quartz schist, and mica schist while the sedimentary rocks consist of Upper Cretaceous sediments (sandstone, ironstone, and siltstone) which are believed to be between 300 m to 1000 m thick. (Ajadi et al., 2015) closely relate a series of parallel subsidiary shear zones that are associated

with regional lineaments, the spatial and temporal associations existing between gold mineralization and quartz-filled shear zones that suggested the gold mineralization is structurally controlled with emplacement of which is regionally consistent with NE-SW and NW-SE fissure directions but with no lithological preference.

The aim is to delineate prospective sites for gold exploration through integrated analysis of hydrothermally altered zones, lithological characterization, and lineament structural analysis using airborne geophysical data (Magnetic and Radiometric).

Location and Geology of the study area

The study area covers Lafiagi (Sheet 203) in the Nigerian topographical map. It covers the towns of Lafiagi, Gbugbu, Lema, Ndeji, Lata, Oke-Ode, Dumagi, Zambufu, etc (Fig. 1a). It is bounded by latitudes 008^0 30′ N to 009^0 00′ N and longitude 005^0 00′ E to 005^0 30′ E. The land area covered ½ degree by ½ degree contour map on a scale of 1:100,000 with topographical elevation ranging from 48 m in the valleys to 484 m on the hills as shown on the digital elevation model (DEM) in (Fig. 1b), with the lowest value occupying very little space (light blue to dark blue) found in the NNE part of the area indicating sedimentary terrain and moderate to highest value occupying other portions of the area. The topography and landscape of the area can generally be described as gently undulating to steep but in some areas is punctuated by hilly ridges consisting of gravel, lateritic soil, alluvial soil, clay, sandy clay, and topsoil and low-lying outcrops at the lowland area. Vegetation is of Guinea savannah type and the climate is of humid tropical Guinea type which, according to Udo (1982) has a characteristic mean annual temperature of 29^0 C and mean annual rainfall of 1300 mm.

Agriculture is the main source of employment and income generation venture for the majority of the inhabitants in the area North Central Nigeria is a component of an Upper Proterozoic mobile belt that crosses the southern Sahara from Algiers into Nigeria, Benin, and Cameroun. This Pan-African belt continues into Northeast Brazil where analogous rare-metal mineralized pegmatites are also known (Garba, 2002). They host most of the economic minerals in the Basement Complex. The end of the Pan-African tectonic event is marked by a conjugate fracture system of the strike-slip faults (Ball, 1980). Fault directions have consistent trends and sense of displacement; i.e a NE-SW (NNE-SSW) trending system has a dextral sense of movement and a NW-SE trending system a sinistral sense (McCurry, 1971; Wright, 1976; Ball, 1980)..

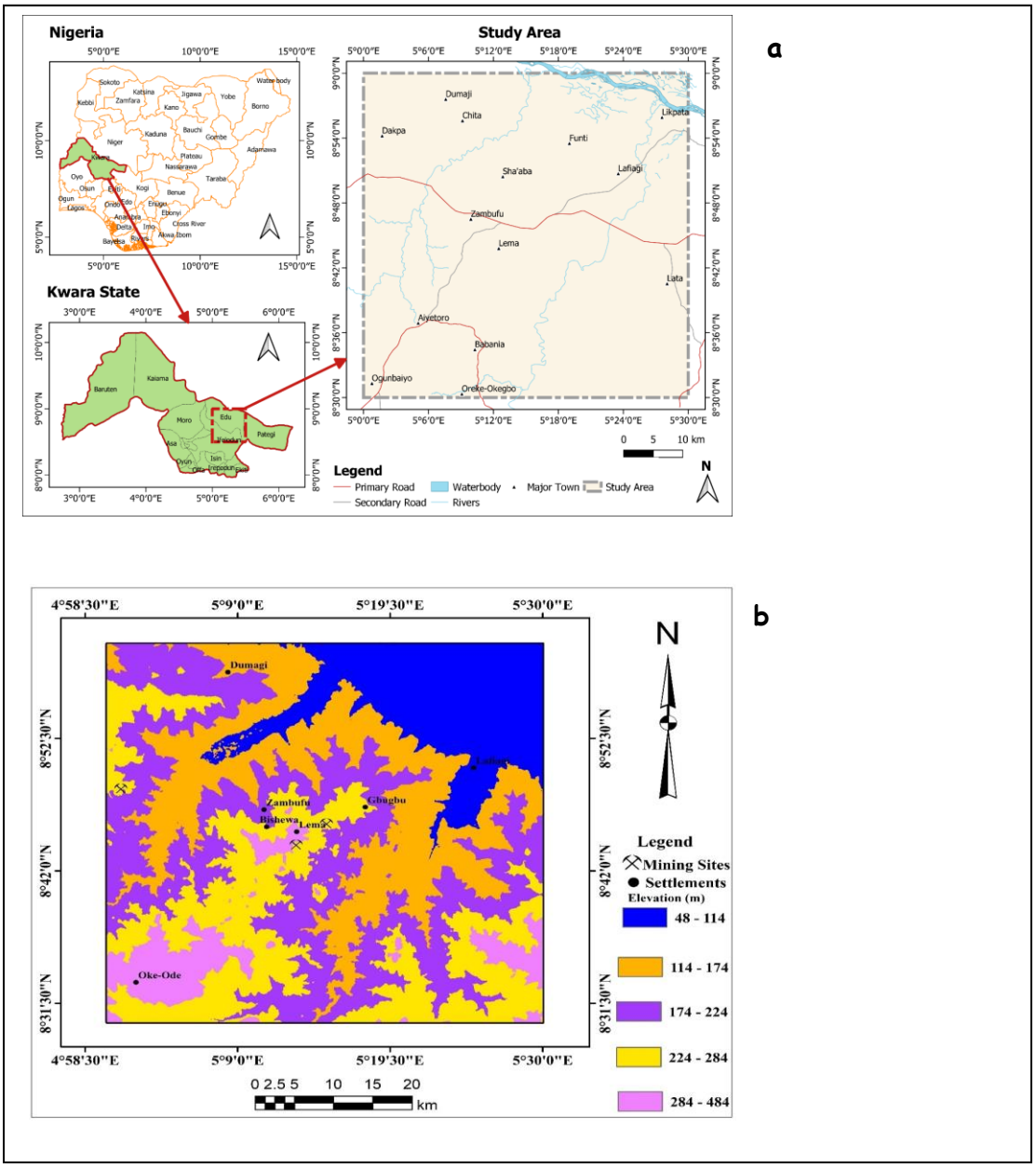

Figure 1: **a** Study and overview area map and **b** Shuttle Radar Topographic Mission (SRTM) Digital Elevation Model (DEM) map of the study area.

The area under study lies in a transition environment between the Nupe Basin and the Southwestern Nigerian Basement Complex with the mining sites in the Basement region of the study area (Fig. 2). Generally, the Basement Complex rocks of Nigeria comprise four major lithological units namely; Migmatite-gneiss complex, Schist Belt, Older Granite, and Undeformed acid and basic dykes. The Basement rock types within the area include granites, biotite gneiss, amphibolite, quartz schist, and mica schist with high percentage of granitic rocks. The Sedimentary rocks consist of Nupe sandstone of Upper Cretaceous sediments (sandstone, ironstone and siltstone) which are believed to be between 300 m to 1000 m thick (Adeleye, 1973)

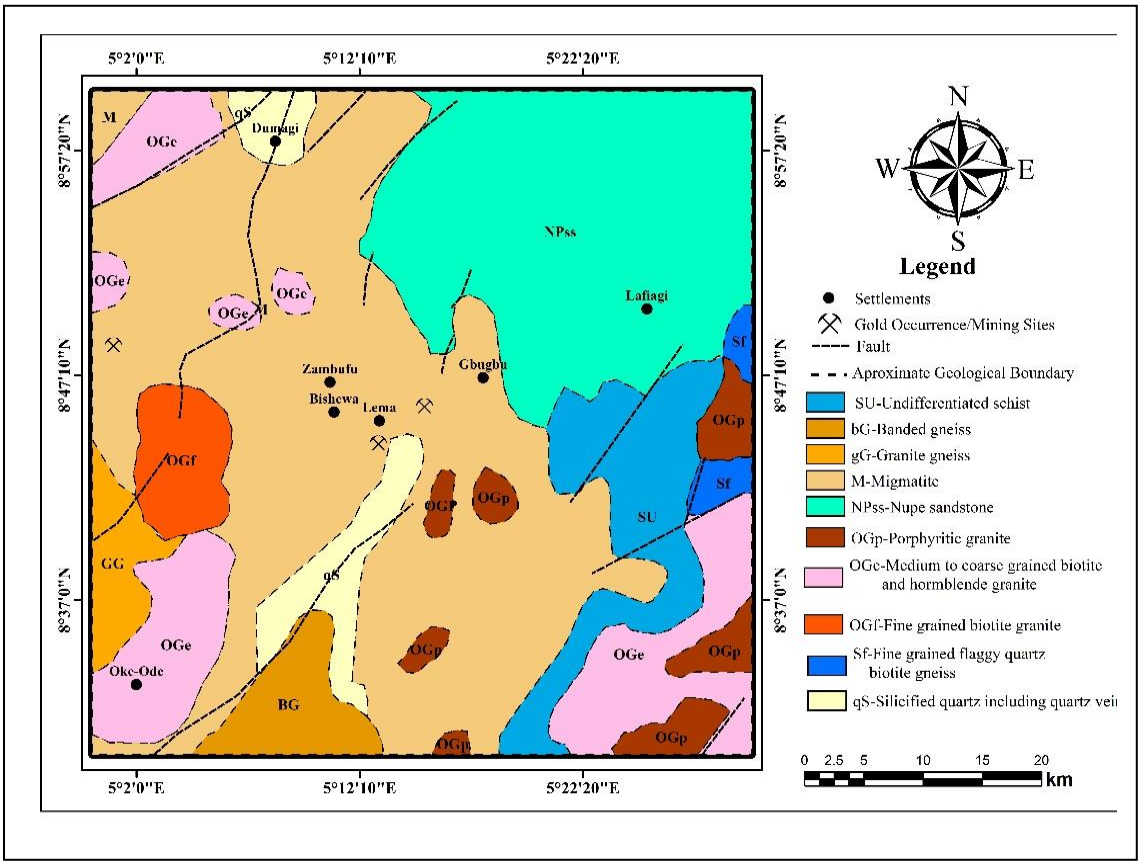

Fig. 2 Geological Map of the Study Area (After NGSA,

Mineralization

The Schist Belts of the Basement Complex rocks have been reported to host the most gold mineralization in Nigeria (Obaje, 2009). However, the gold distribution pattern within the region exhibits a lack of lithologic preference, and the gold-bearing veins are similar to the auriferous quartz veins of the Okolom and Ilesha gold fields (Ajadi et al., 2015; Aliyu, 2020b). The study area is an integral part of the northwestern extension of the Okolom-Dogondaji gold field (Aliyu, 2020b). Additionally, the Ifewara fault zone (which is one of the four most important fault systems in Nigeria) cut across the study area.

Materials and Methods.

Data Acquisition

High-resolution airborne geophysical data (magnetic and radiometric) used in this research were acquired from Nigeria Geological Survey Agency (NGSA). The survey ran from 2005 to 2009 using aircraft along a series of NW – SE flight lines with a line spacing of 500 m and an average of 80 m terrain clearance. For the aeromagnetic data, regional/residual separation was performed on the Reduction to Equator (RTE) of Total Magnetic Intensity (TMI) (Fig. 3a) using International Geomagnetic Reference Field (IGRF) 2005, the residual data (which is of interest) was utilized for further processing (Fig. 3b).

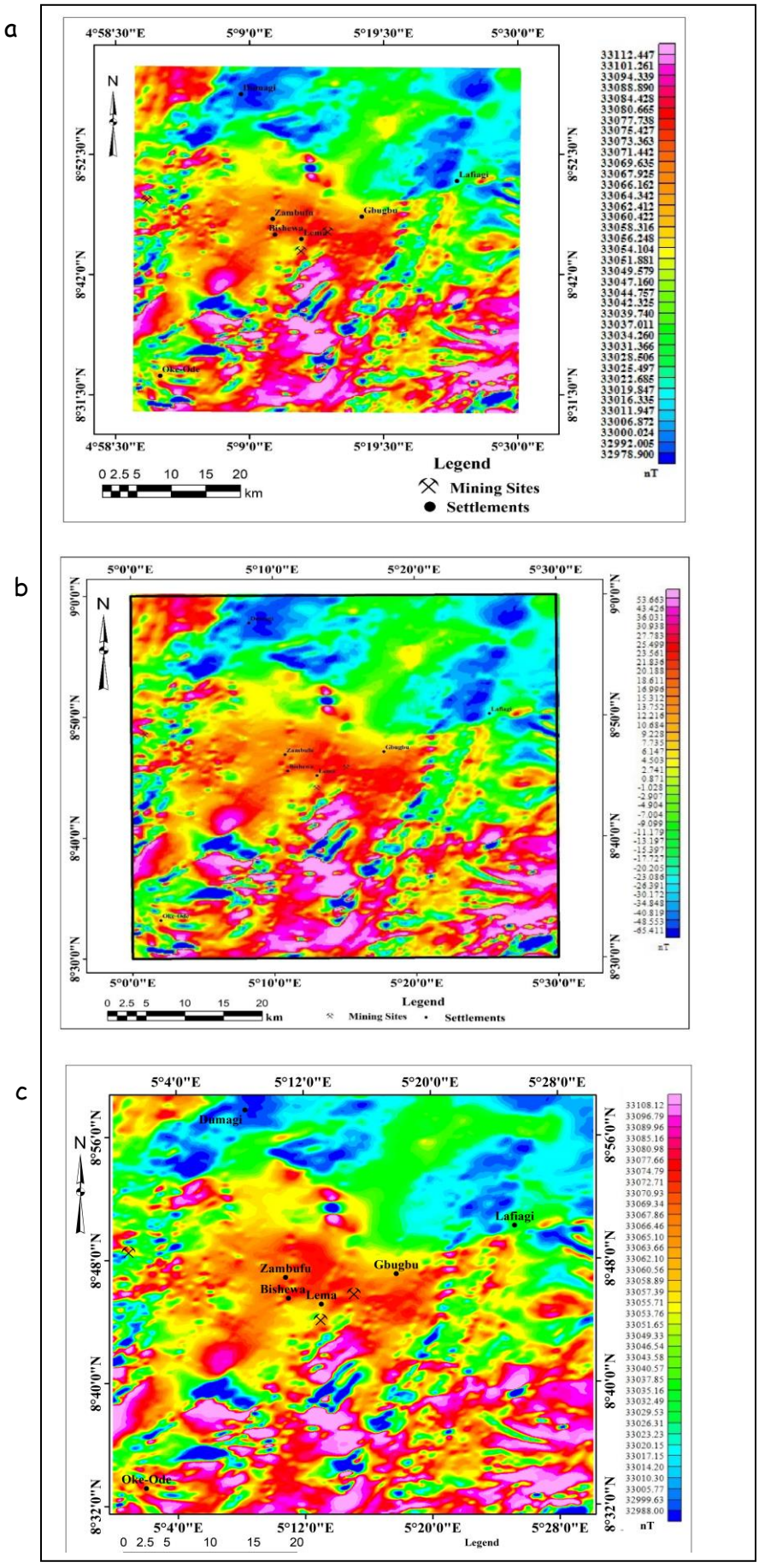

Figure 3: (**a**) Total Magnetic Intensity (TMI) map (**b**) Residual map (**c**) Reduction to Equator (RTE) of the study area

Because the geomagnetic field's inclination and declination vary from the equator to the pole, reduction to the equator (RTE) correction was applied to the aeromagnetic anomaly data (Fig. 3c). As a result, the peak of the total magnetic anomalies caused by the subsurface is no longer directly over the source. By making use of this, the shape and peak of the magnetic anomalies over their causative sources are corrected for spatial shift, which in turn improves the precision of the analysis (Hinze et al., 2013; Lawal, 2020; Elkhateeb & Abdellatif, 2018a). Aeroradiometric data were procured in grid form of equivalent Uranium (eU) and Thorium (eTh), Potassium in percentage (%K), and Total count (TC). They were subjected to some enhancement techniques and further processing was carried out using Oasis Montaj Software.

Data Processing

Aeromagnetic data processing

The resulting RTE map reveals the magnetic intensity distribution within the study area with maximum amplitude values of roughly 33108.12 nT (Fig. 3c). The areas of maximum amplitude are the southern part of the study area which corresponds to area dominated by the basement rocks. The following signal enhancement techniques are applied to the RTE in order to better understand the mineralization of the area.

First Vertical Derivatives (FVD)

A good representation of features closer to the subsurface, such as faults is enhanced upon the application of FVD filtering technique. In this instance, data filters improved high-frequency anomalies, allowing shallower sources to be mapped at the expense of low-frequency ones(Okeyode et al., 2019; Aliyu et al., 2020b; Eldosouky et al., 2022). FVD was first used by Evjen (1936) to delineate edges of gravity and magnetic bodies using equation one where M represents the magnetic field, and z represent the z-direction (Ibraheem et al., 2019).

$$FVD = \frac{\partial \mathrm{M}}{\partial z} \quad (1)$$

Analytical Signal (AS)

The analytical signals filter does not depend on the geomagnetism field direction (inclination and declination) of the host body. As such direct maximum can be produced over discrete bodies and their edges using analytical signals in both the frequency and spatial domains. Analytical signal as an enhancement technique which is used related to magnetic field from the three orthogonal derivatives using equation 2 was used for delineation of edges of geologic bodies; (Ibrahim et al., 2019)

$$\mathrm{AS}\ (x,y) = \frac{\partial M}{\partial x}\hat{x} + \frac{\partial M}{\partial y}\hat{y} + i\ \frac{\partial M}{\partial z}\hat{z}, \quad (2)$$

where AS(x,y) is the AS amplitude at (x,y).

Centre for Exploration and Targeting (CET) Enhancement Techniques.

In order to map structural complexity (SC) zones for investigation, the CET grid analysis technique is important to improve the texture of the magnetic signatures. The technique of SC is used to identify zones where mineral deposits are likely to develop or occur (Eldosouky et al., 2017, Holden et al., 2010). The CET approach combines the identification of two-sided symmetric points and texture analysis to find discontinuities in magnetic data (Kovesi, 1991; Holden et al., 2010;

Eldosouky et al., 2017). Both texture enhancement using standard deviation to identify the regions of complex textures connected with discontinuities in magnetic data and phase symmetry in identifying areas of lateral discontinuity as in equation 3

$$SD = \sqrt{\left[\frac{1}{N}\Sigma(x_i - \mu)^2\right]} \quad (3).$$

Magnetic Susceptibility (K)

When there is no external magnetic field, individual magnetic zones (magnetic domain) within rocks, soils, or other minerals will be generally oriented randomly. The net effect would be a zero magnetic field. The physical characteristic known as magnetic susceptibility describes how much a material can be magnetized under an applied external field (Dalan, 2006). Magnetic susceptibility is one attribute of a particular mineral type in geology. The kind and quantity of minerals in the sample are revealed by its measurement. The amount and composition (shape and size) of iron oxide in the rocks serve as sole indicators of magnetization (Dearing, 1994; Wemegah et al., 2009). The magnetic susceptibility effectively is the magnetization effect divided by the applied magnetic field. If the magnetic field is **H** (A/m) and the magnetization is **M** (A/m), the magnetic susceptibility is;

$$k = X_v = \frac{\boldsymbol{M}}{\boldsymbol{H}} \quad (4)$$

where X_v is the volume of susceptibility

Theory of Euler Deconvolution

It is founded on the Euler homogeneity; equation 4 given by Thompson (1982) which connects the potential field's (gravity or magnetic) gradient components to the sources' locations via the degree of homogeneity N, also known as a structural index. Sources are simple geometrical object such as a homogenous point source $N = 3$, a linear source (line of dipoles or poles, and for a homogenous cylinder, rod, etc.) $N = 2$, for intrusive bodies (thin layer, dyke, etc.) $N = 1$, for a contact, vertex of a block and a pyramid with a big height $N = 0$. The choice of a proper SI is a function of the geometry of causative bodies. Estimation of the correct structural index is crucial for the successful application of the Euler deconvolution method (Reid *et al.*, 1990). And this is achieved by using the index that produces the best clustering of solutions (Reid, 1995).

$$(x - x_0)\frac{\partial T}{\partial x} + (y - y_0)\frac{\partial T}{\partial y} + (z - z_0)\frac{\partial T}{\partial z} = N(B - T) \quad (5)$$

where (x_0, y_0, z_0) is the position of a magnetic source whose total field T is detected at (x, y, z). The total field has a regional value of B.

Aeroradiometric Data Processing

The radiometric method operates on the assumption that radioactive elements occur naturally in the crystals of particular minerals, the abundance of these minerals varies across the Earth's surface with changes in rock and soil type, and because the energy of gamma rays is characteristic of the radioactive element, it can be used to measure the abundance of these radioactive elements in an area. In this investigation, processing techniques including color composite of grided equivalent Uranium (eU), equivalent Thorium (eTh), percentage potassium (%K), and ratio maps were used to suggest to a great extent the lithological differences due to the colour variations. The uranium, thorium, and potassium maps emphasize regions where the specific radioelement has a total and pretty

higher amount (Aliyu et al., 2020a; Silva et al., 2003). In order to expose the intensities of the three radioelements (Uranium, Thorium, and Potassium), the primary colors red (R), green (G), and blue (B), were modulated in equal ratios to produce a ternary map using Oasis Montaj Geosoft. The lithological disparities through geological and mineral exploration can be understood from this map (Lawal, 2020, Tawey et al., 2021, and Aliyu et al., 2022a).

Results and discussions

First Vertical Derivative (FVD)

The vertical derivative map provides a sharper image than the total magnetic and residual field intensity map because it responds to local impacts much more than wide or regional effects (Cooper and Cowan, 2008; Lawal, 2020; Aliyu et al., 2022b). As a result, small anomalies are easier to see in regions with significant regional disruptions. It displays long and short linear features (Pink and Blue lines) distinguishing the edges of magnetic source bodies with zero contour lines representing the locations of the contacts or faults. The long linear features, which are continuous and less prominent trends in the NE–SW direction, represent lithological boundaries and could be interpreted as major fracture/fault lines within the study area, while the short linear and curvilinear features with their orientation trending mostly NE-SW, NW–SE and N–S are also concentrated within the lithological boundaries of magnetic source bodies of muscovite schist and band granite gneiss (Fig. 4).

Analytical Signal (AS)

The AS map was created using AS grid computed using the first-order vertical derivative values of two horizontal gradients and one vertical gradient of the magnetic intensity. Three main magnetic domains are noticeable on the AS map (Fig. 5) and have high magnetic intensity (HMI) domains with gradient values ranging between 0.085 and 0.257 nT/km, which can be seen in the SSE, SSW, W, and NW corner of the study area; an intermediate magnetic intensity (IMI) with gradient values ranging from 0.025 to 0.077 nT/km; and the last is the domain with low magnetic intensity (LMI) having gradients between 0.004 and 0.024 nT/Km. The majority of geologic bodies possessing high magnetic gradients are trending in the NE–SW direction, while minimum gradients are observed to be trending in the NW–SE direction. Regions with high magnetic gradients are linked to an intrusive granitic body that is rich in ferromagnesian-bearing rocks and contains few felsic minerals, such as porphyritic granite, medium- or coarse-grained biotite granite, hornblende granite, and granite gneiss (Telford et al. 1990; Ahmed 2018; Balogun 2019). On the other hand, the low and intermediate-magnetic intensity zones could be reflections of downfaulted sediment-filled basement or perhaps a group of tectonic trends that are in charge of the sediments above them. Rocks associated with these zones contain more than 60% quartz, so they are identified as metavolcanic, metasediments, and granites (Telford et al. 1990; Ahmed 2018). The map also shows networks of magnetic discontinuities that might represent fracture zones that could be targeted for mineral prospection

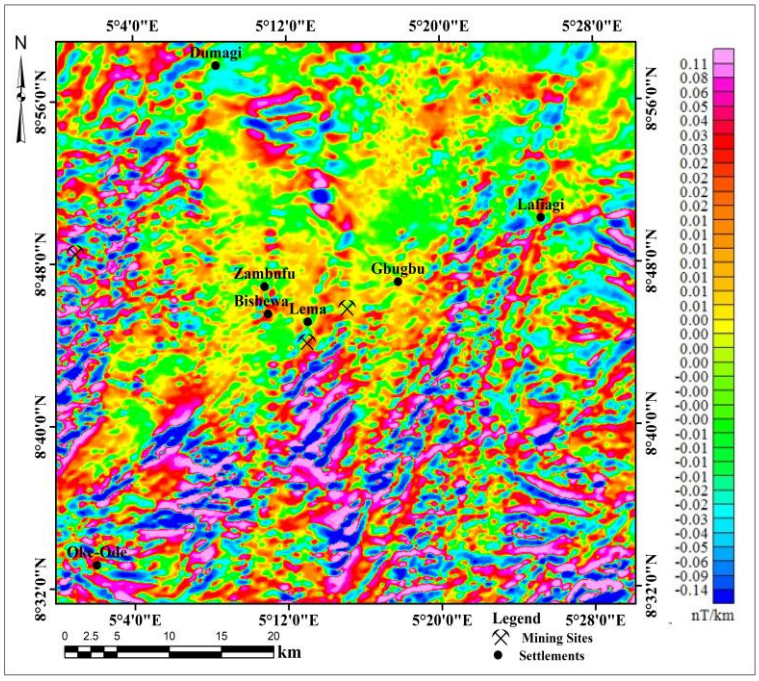

Fig. 4: First Vertical Derivative (FVD) Map of the Study Area

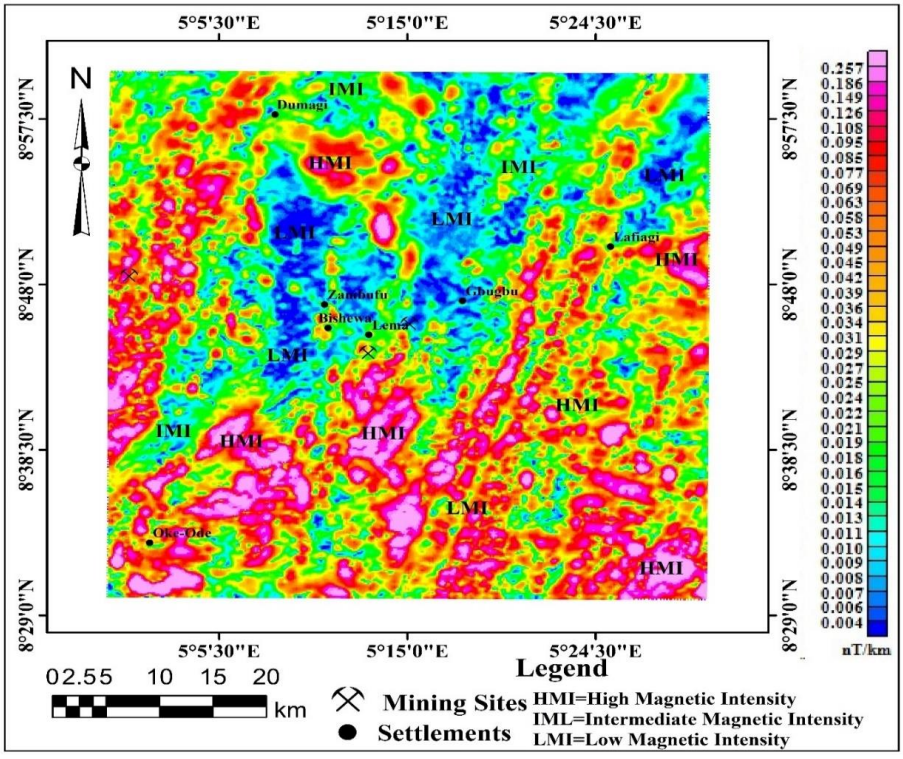

Fig. 5: Analytical Signal Map of the Study Area

CET grid Analysis

The CET grid analysis was applied to the RTE map to identify linear structures, it calculates magnetic variations, and phase symmetry to detect any regions of lateral continuity or otherwise, amplitude thresholding was used to improve lineaments by filtering out background and noise signals(Eldosouky et al., 2020; Lawal, 2020; Umaru et al., 2022a. CET grid analysis produces a vectorization map (Fig. 6) that reveals lineament features that correspond to structures, such as faults and fractures, lithological boundaries, and buried ores that demonstrate how the basement rocks in the region are controlled structurally. The principal structural lineaments trends NE-SW, and other features trends in the NW-SE, E-W, and N-S directions. These trends are associated with the effects of the Earth's deep heterogeneity, granitic and metasediment rocks which are represented by fractures and faults that affect the basement complex or both the basement and the overlaying sediments (Balogun 2019; Aliyu et al., 2020b). A rose diagram (Fig. 7) depicting the region's orientation pattern as NE-SW, NW-SE, W-E, and N-S was produced using the orientation deduced in the lineament map having the same pattern as in the grid analysis map. The lineament map indicates structural characteristics that correspond to faults and fractures that could be potential hiding places for ore minerals or conduits for ore fluids to be routed to spots of deposition.

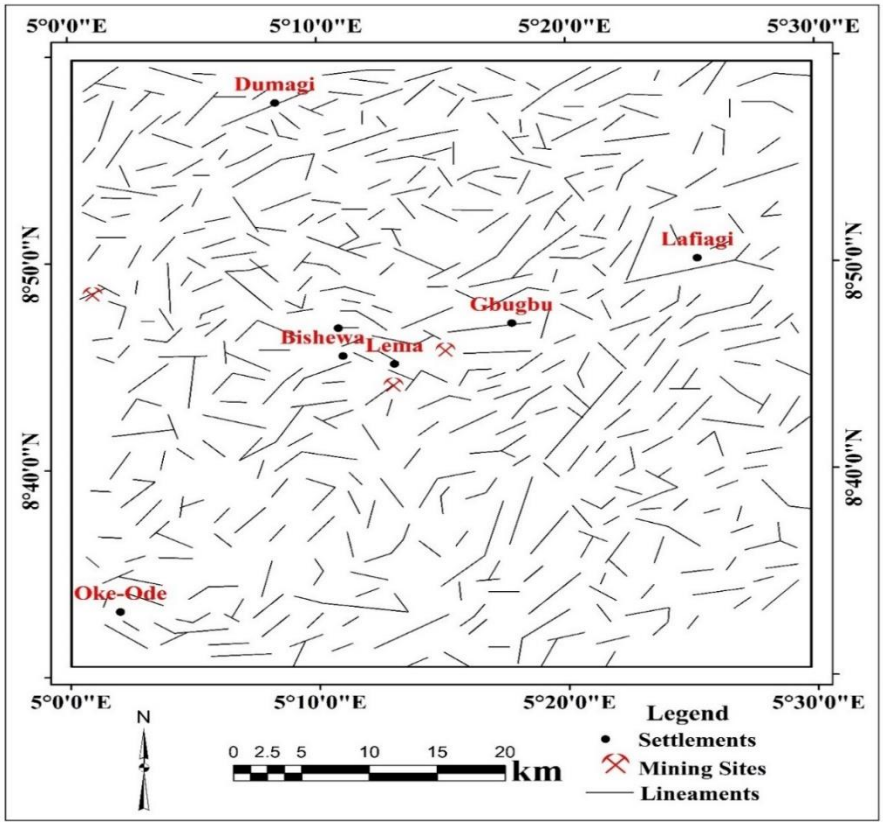

Fig. 6: Lineament Map of The Study Area

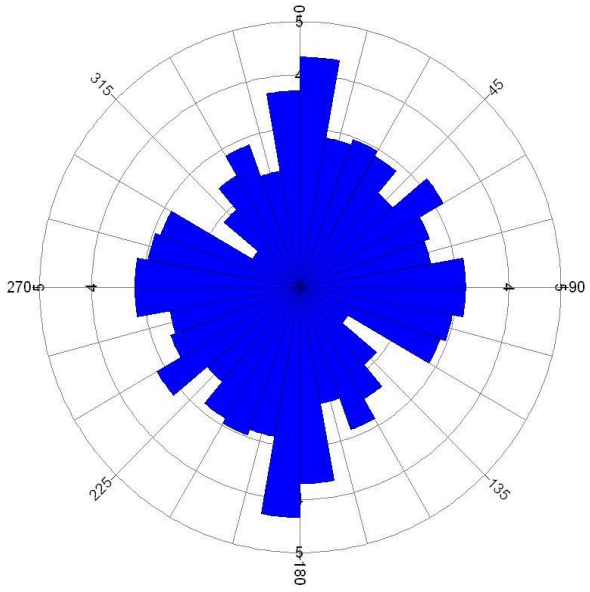

Statistical Summary

Calculation Method:	Frequency
Class Interval:	10.0 Degrees
Min.Length Filtering:	Deactivated
Max.Length Filtering:	Deactivated
Azimuth Filtering:	Activated
Minimum Azimuth #1:	0.0 Degrees
Maximum Azimuth #1:	360.0 Degrees
Minimum Azimuth #2:	0.0 Degrees
Maximum Azimuth #2:	360.0 Degrees
Data Type:	Bidirectional
Rotation Amount:	0.0 Degrees
Population:	473
Total Length of All Lineations:	1,386,345.65
Maximum Bin Population:	41.0
Mean Bin Population:	26.28
Standard Deviation of Bin Population:	6.5
Maximum Bin Population (%):	4.33
Mean Bin Population (%):	2.78
Standard Deviation of Bin Population (%):	0.69
Maximum Bin Length:	61,820.86
Mean Bin Length:	38,509.6
Standard Deviation of Bin Lengths:	10,680.63
Maximum Bin Length (%):	4.46
Mean Bin Length (%):	2.78
Standard Deviation of Bin Lengths (%):	0.77
Vector Mean:	28.5 Degrees
	208.54 Degrees
Confidence Interval:	17.1 Degrees
	(80 Percent)
R-mag:	0.14

Fig. 7: Rose diagram for lineaments showing orientation of structures within the study area

CET Porphyry Analysis

Porphyry-like intrusions are circular or semi-circular structures with zones of weakness at their rims or boundaries that aid in the ascent of hydrothermal solutions (Elkhateeb and Abdellatif 2018). Here, these intrusive features show a unique correlation with the fracture zones (lineaments) extracted from the CET grid structural map which links the locations of porphyry intrusion that represents the preferred orientation for ore deposition and indicates a substantial likelihood of additional mineral occurrences in the study area along these trends, these intrusive features together represent the area's point of reference for its mineral potential. Also, these show how magnetic highs and basement rocks primarily influence porphyry intrusions. The accurate mapping of new areas with a high probability of gold mineralization was made possible by the good agreement between known mineralization locations and interpreted structures, structural complexity, and porphyry density maps. Consequently, the majority of porphyry intrusions existed within the basement complexes showing good correlation with analytical signal, first vertical derivative and Euler deconvolution depth solution trend maps (Fig. 8 and 9).

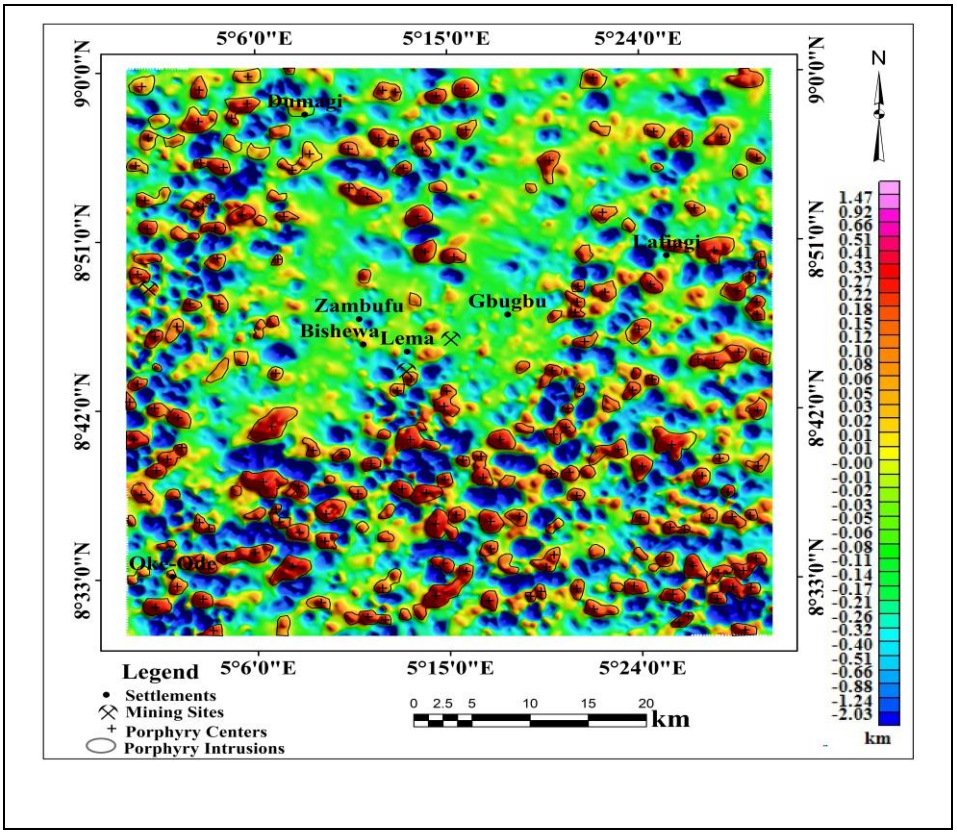

Fig. 8: CET Porphyry Intrusion Boundary Enhancement Map

Susceptibility

The relevant physical property for magnetic surveys is magnetic susceptibility, or less frequently, the related property magnetic permeability. The apparent magnetic susceptibility values were estimated using the filter operator in Oasis Montaj™ giving apparent susceptibility values ranging from -0.0007 to 0.0007 as shown in (Fig. 10). The map revealed high, intermediate, and low magnetic susceptibility. Regions of high susceptibility range from 0.0002 to 0.0008 SI units associated with igneous rocks of high ferromagnetic minerals such as magnetite, hematite, and intermediate susceptibility values ranging from -0.0001 to 0.0001 SI units associated with ilmenite, pyrite, pyrrhotite, quartz, rock Salt, and calcite minerals while low susceptibility values range from -0.0008 to -0.0002 SI unit mostly associated with some metamorphic and sedimentary rocks (Teford *et al.*, 1990). Most associated igneous rock with susceptibility between 0.0002 and 0.0008 trends NE-SW, inferred to be a conduit for alteration zones.

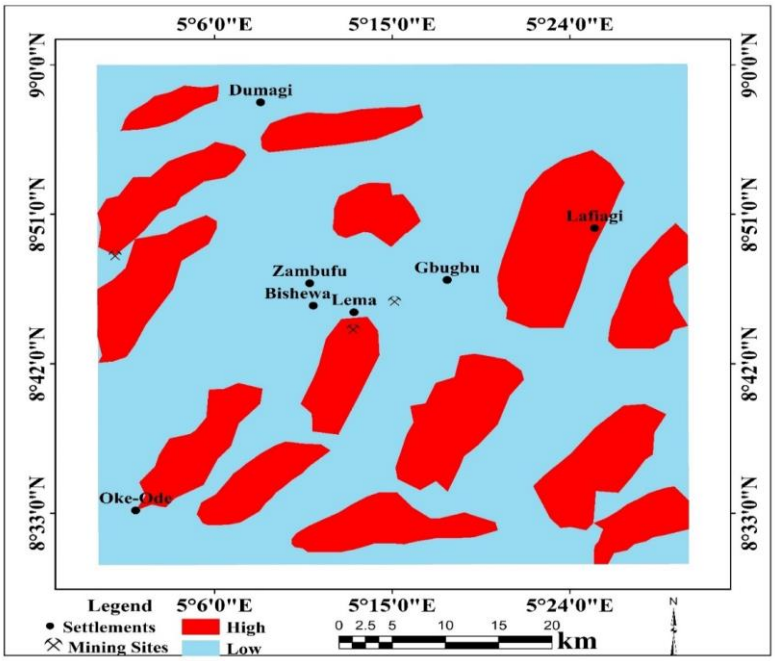

Fig. 9: Density Map of Porphyry Intrusion

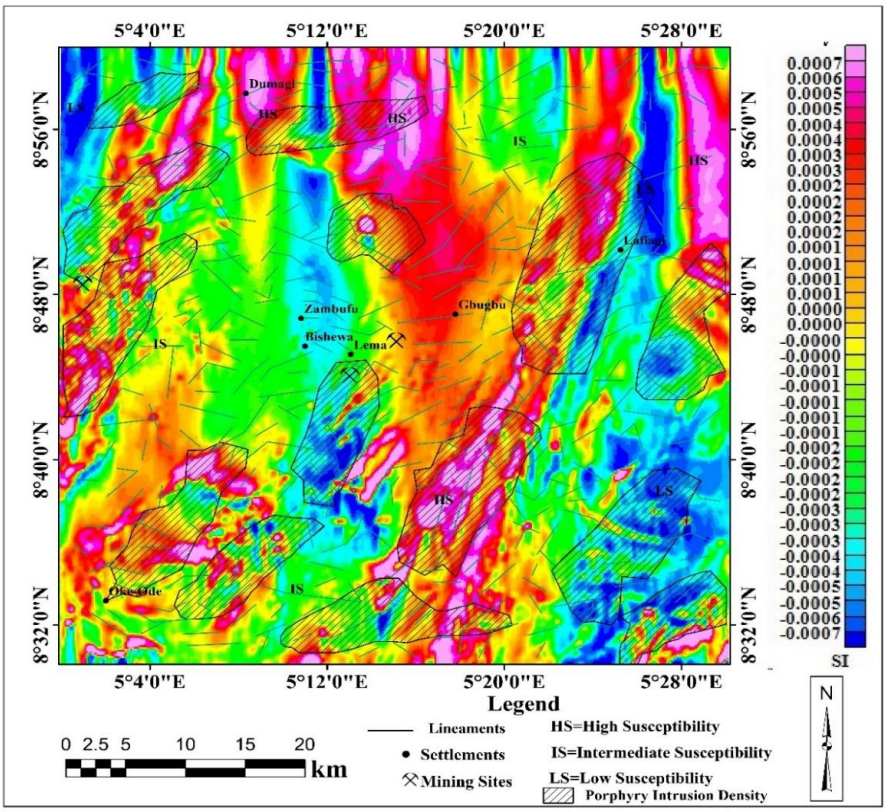

Fig. 10: Lineament and Porphyry Density overlay on the Susceptibility

Euler Deconvolution

The Euler deconvolution method of depth determination is an automatic technique used for locating the source of the potential field based on amplitudes and gradients. The Euler deconvolution algorithm was implemented to the gridded residual field intensity map to generate and locate the solution source of the magnetic field. Several structural indices ranging from 0 to 3 were tested but the structural index of 1.0 provides consistent solutions and found to agree with that of a dike model attributed to being fractures filled with fluid materials. These fluid materials are inferred to be gold contents within the fractures. The resulting map was superimposed on the grey residual grid (Fig. 11) giving the position, depth, and boundaries or contact of the location of anomalous magnetic sources. Most solutions aligned within and along fracture and lineament trends of predominant NE-SW and NW-SE ranging from 100 m to 1000 m indicating a shallow source.

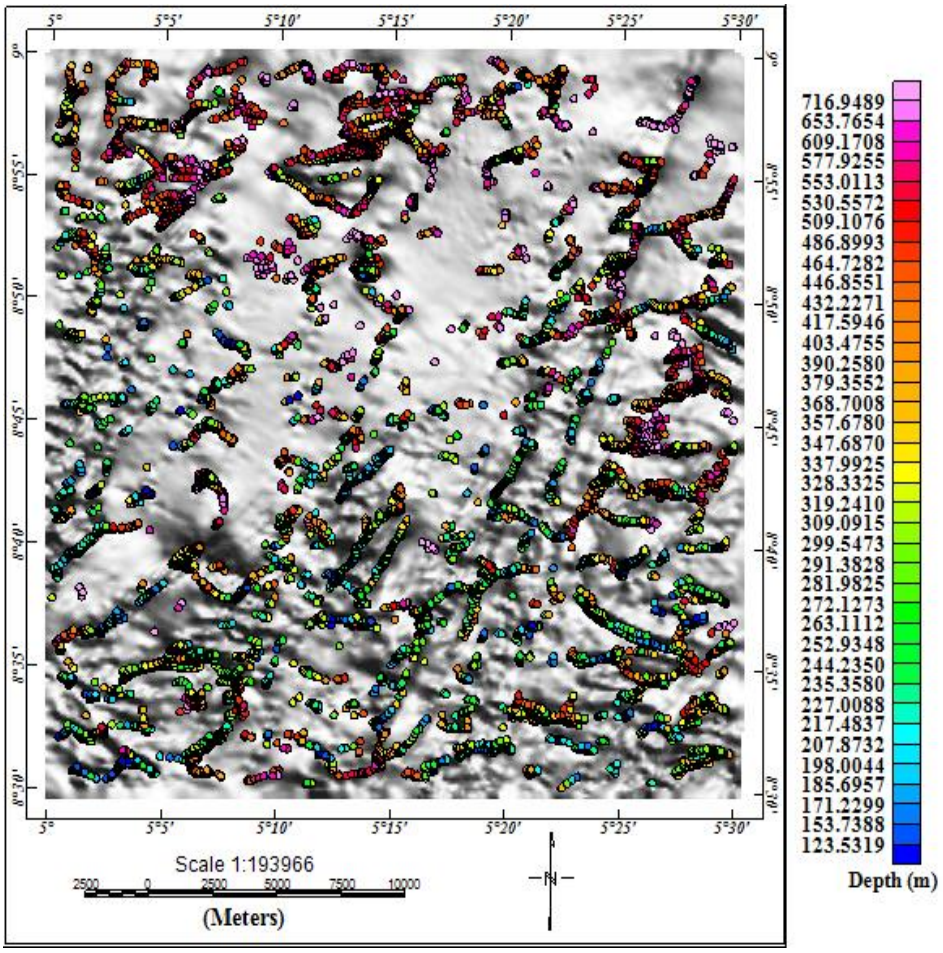

Fig. 11: Depth to Magnetic Basement of the Study Area

Total Count (TC), Percentage concentration of Potassium (%K), Equivalent Thorium (eTh), and Equivalent Uranium (eU).

The radiometric survey data produced the various radioelements; potassium (K), uranium (U), and thorium (Th) anomalies. The resultant anomalies are being interpreted as total count (μR/h). Total Count (TC) (Fig. 12) has regions with high concentrations ranging from 2768.806 to 4619.800 μR/h around Northeastern, Southeastern, and Southwestern areas, associated with granitic rocks, intermediate to low concentration range from (1232.680 to 2537.400 μR/h) and (669.119 to 1176.503 μR/h) respectively. They are associated with metasediments (phyllites), porphyroblastic gneiss, and metavolcanics (amphibolite). Moreso Igneous rocks, such as granite, are reported to have higher radiation levels, while metasedimentary or sedimentary rocks have lower radiation levels (UNSCEAR, 2000). Potassium map (Fig. 13) depicted regions with highest percentage concentration ranging from (2.0475 to 3.6543 %) that correlated to granites and gneisses, low to intermediate concentrations range from (0.1159 to 0.4475 and 0.5011 to 1.8952 %) respectively. These regions are associated with metavolcanic, meta-gabbro, and carbonate rocks.

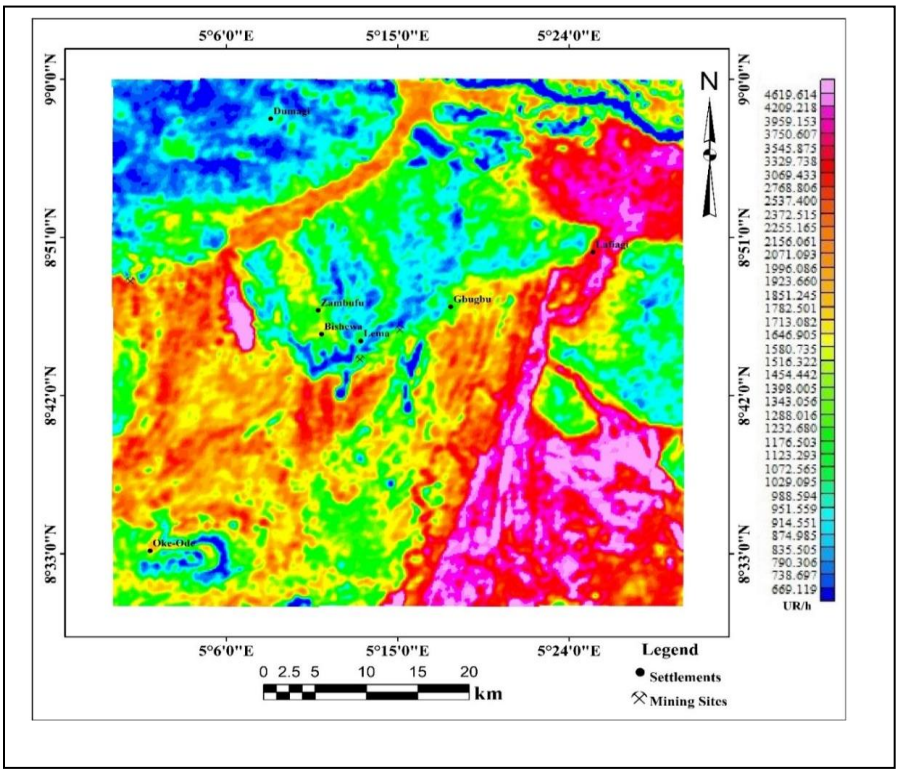

Fig. 12: Total Count Map of the Study Area

For the equivalent thorium (eTh) map (Fig. 14), a high equivalent concentration level ranging from (13.843 to 50.041 ppm) is associated with metavolcanics, meta-gabbro, and talc

carbonate rocks, while an intermediate concentration level ranging from (8.299 to 13.207 ppm) and a low concentration level ranging from (2.584 to 7.788 ppm) are associated with metasediments and metamorphic rocks

High concentration levels on the equivalent uranium (eU) map (Fig. 15) which ranges from 21.539 to 38.061 ppm covering northeastern, southeastern, and western regions are connected to granitic rocks and metamorphic rock. The low concentration levels range from 5.066 to 8.810 ppm, and the intermediate concentration levels ranges from 9.028 to 20.110 ppm are associated with metavolcanics, metasediments, and metagabbro.

K(%)/Th(ppm)

The Potassium-Thorium ratio map (Fig. 16) is crucial for delineating structures connected to hydrothermal alteration zones since high concentration of Potassium and low concentration of Thorium are related to modifications in many ore deposits (Ostrovskiy, 1975; Elkhateeb and Abdellatif, 2018; Bukola et al., 2021 and Aliyu et al., 2022a). The K/Th ratio map depicted hydrothermal process-affected regions in red to pink color (0.124-0.405 %/ppm strong indicator). As observed on the map, most of these alteration zones are trending in NE-SW directions that are in the same pattern with delineated structures using enhanced aeromagnetic data, these regions are most prominent in the Southwestern and prominent in the Southeastern of the study area. These regions are associated with coarse-grained biotite, hornblende granite, and granite gneiss.

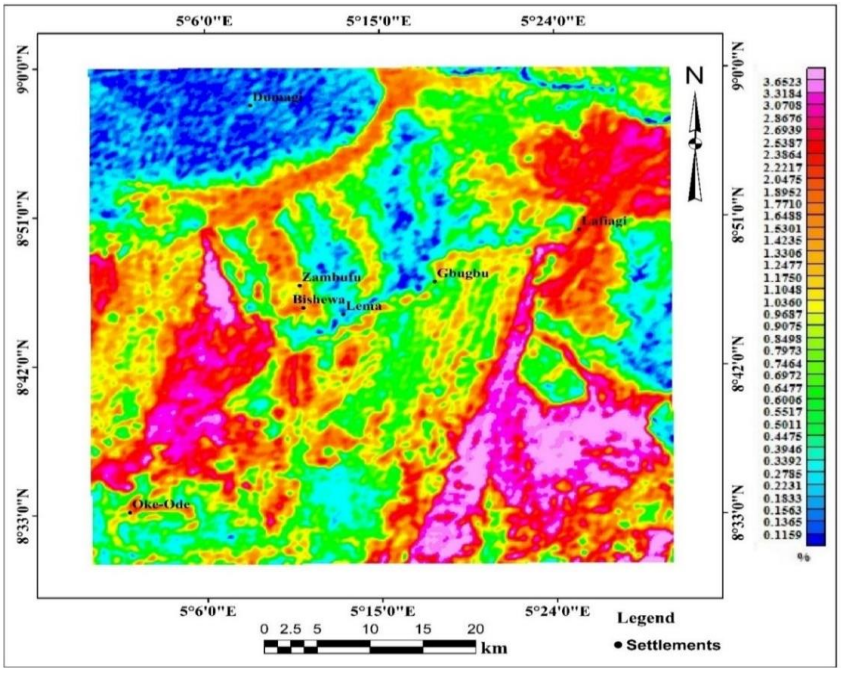

Fig. 13: Percentage Concentration of Potassium (%K) Map of the study

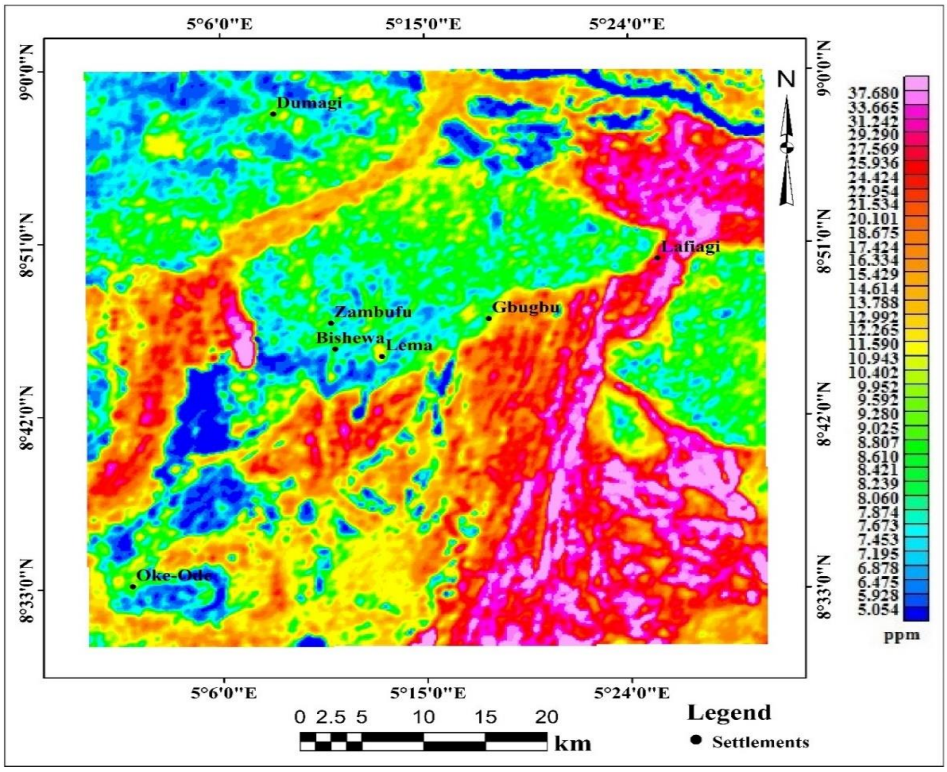

Fig. 14: Equivalent Thorium (eTh) Map of the Study Area

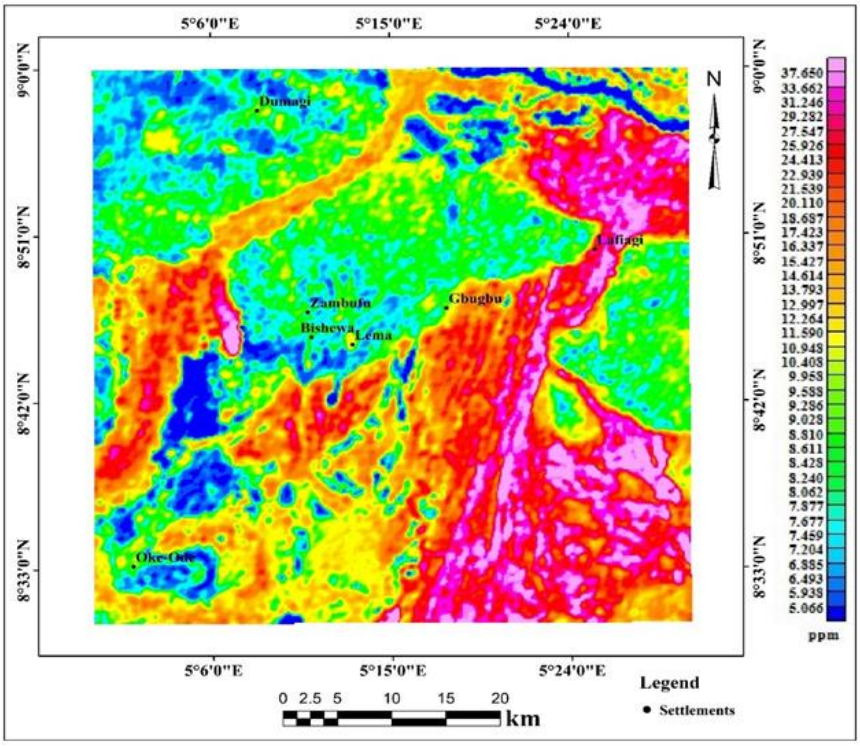

Fig. 15: Equivalent Uranium (eU) Map of the Study Area

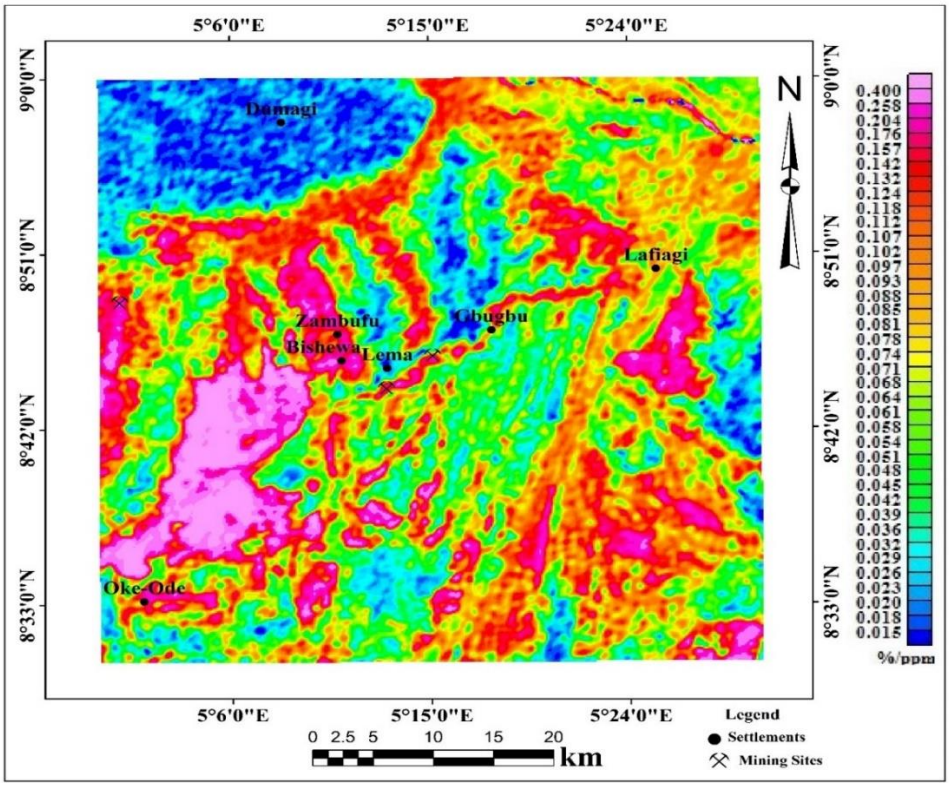

Fig. 16: Potassium/Thorium Map of the Study Area

Ternary Map

The ternary radiometric map is a unique representation of surface to near-surface geological units or boundaries. The lithological disparities through geological and mineral exploration can be understood from this map (Lawal, 2020; Tawey et al., 2021; Aliyu et al., 2022a). The ternary map (Fig. 17) displays high concentrations of radioelements characterized by white colors, and these regions/zones are represented by grained biotite, hornblende granite, and granite gneiss. They represent promising targets for the exploration of radioactive minerals (Tawey et al., 2021). Amphibolite and Metavolcanic rocks, which are indicative of regions with low radioactive element concentration, exhibit black to brown colors, the red color reflects high K content but low Th and U related to granitic and metasedimentary rocks. The green hue refers to regions of high Th, low K, and U linked with metavolcanic rock formations. Regions with yellow colors are connected with fine-grained granitic rocks because of their high potassium and thorium with low uranium concentrations.

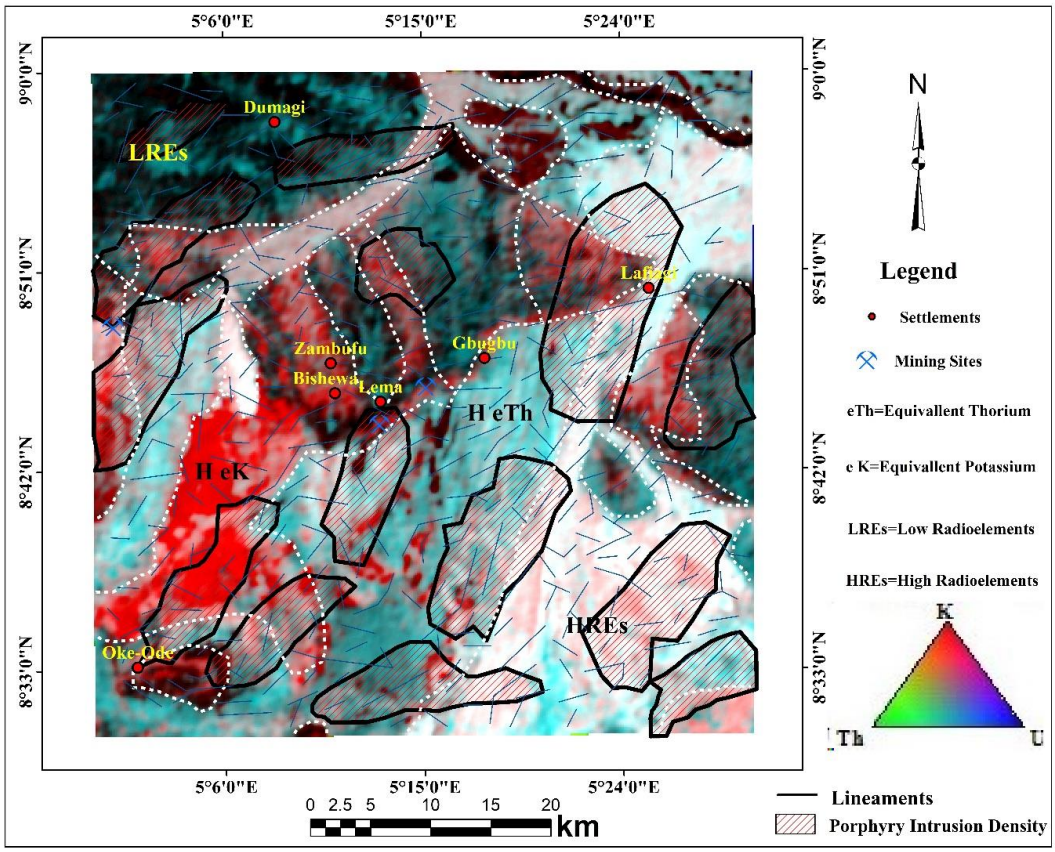

Fig. 17: Lineament and Porphyry Density overlay on the Lithological Ternary Map.

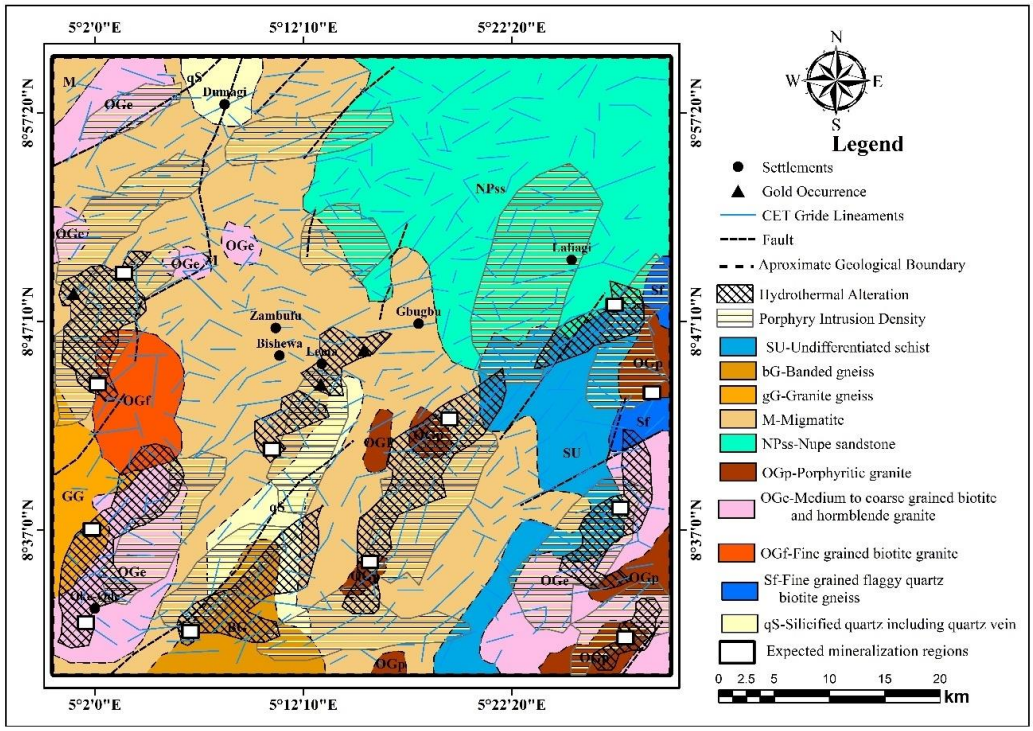

Fig. 18: Composite Map of Aeromagnetic, Aeroradiometric, And Geology with Known Gold

Integration and Interpretation of Airborne Geophysical data

The geophysical analysis technique's strategy of correlating several data is important for mapping mineral potential in that, different lithological units and associated geological structures were inferred from the integrated airborne geophysical datasets that aided in predicting and delineating potential zones that could be possible hosts to gold mineralization.

The mapped geological structures, lithology, and hydrothermal alteration zones are the key parameters considered for the integration. From the interpreted structural maps, the structural trends are NE-SW, N-S, E-W, and NW–SE. Areas of great structural complexity exhibit fractures that facilitate fluid transport in voids during hydrothermal activity. Boadi et al. (2013).

As such, the predominant geological features in the area trends in NE-SW, which can be interpreted as faults, connecting joints, or shear zones developed during regional NW-SE compression and hence reflect the favoured direction of ore deposit within the area.

Hydrothermally altered zones are often attributed to elevated K. The reason is that K becomes more receptive in the shear zone due to the breakdown of feldspars, biotite, and muscovite in clay minerals. High structural connectivity and areas reflected by moderate to high magnetic anomalies were of much importance. In regions where the two coincide and are also marked by faults, fault intersections, fractures, shear zones, and relative geologic susceptibility were used to map alteration zones due to the possibility of hosting hydrothermal fluids as a result of the intense permeability. The integration of hydrothermally altered zones and delineated structures was used to generate potential mineralization zones in the area

The areas of more surface lineaments and porphyry intrusion densities represent the most appropriate sites for mineralization, which allows for the hydrothermal solutions to deposit their economic minerals along these weak-fractured zones. These surface structures are mainly related to the NW–SE and NE–SW trends. (Fig. 18).

Conclusion

Integration of airborne geophysical data (magnetic and radiometric) of Lafiagi (sheet 203) was analyzed successfully using different and advanced enhancement techniques which allowed the detecting of structural discontinuity and hydrothermal alteration zones (HAZs). Grid transformation techniques including Reduction to the equator, first vertical derivative, analytical techniques, CET grid and porphyry analysis, susceptibility, and Euler convolution depth were performed on aeromagnetic data to reveal variations in magnetic intensity and apparent susceptibility, continuity, or discontinuity in geological body or structures and depth to the causative body while individual radioelement grids, the ratio of K/Th, Total count and ternary map were produced to reveal near surface lithological units, area of HAZs

Structural map derived from the enhancement and CET technique indicate that near-surface lineaments and geologic structures are along NE-SW and NW-SE,

while a few trends in N-S and E-W. These orientations are associated with alteration zones inferred to be gold mineralization spots considering the gold-known mineralized locations within the study area. The distribution of the three radioelements associated with the geological structures of the area has been studied, and it was noted that both uranium and thorium have almost equal concentration distribution across the study area with a difference of 0.030 ppm. The maximum values of eU and eTh (ppm) fall within the undifferentiated schist, grain biotite, biotite gneiss, and Nupe sandstone, while the K (%) have least values compared to others due to its prone to mobility, its maximum values fall within granites and gneisses region. Regions with high values of K/Th ranging from 0.16 to 0.480 %/ppm indicate regions with remarkable hydrothermal alteration zones. The alteration zones of high potassium enrichment, structural trends associated with known gold locations, and apparent susceptibility values were used as basic parameters/guides to infer some prospective zones for gold mineralization within the study area.

Declarations.

The authors declare no competing interests.

References

Adeleye, D.R. (1973). Origin of Ironstones: An example from middle Niger valley, Nigeria. *J. Sedimentary Petrol.*, 43: 709-727.

Ahmed, S.B. (2018). Integration of airborne geophysical and satellite imagery data to delineate the radioactive zones at west Safaga Area, Eastern Desert, Egypt. *NRIAG J Astron Geophys* 7(2):297–308.

Ajadi, J., Adedoyin, A. D., & Bamigboye, O. S. (2015). *Origin and Structural Control of Gold Mineralization in Bishewa Area, Central Nigeria 5 PUBLICATIONS 2 CITATIONS SEE PROFILE*. https://www.researchgate.net/publication/336180566

Akande, S. O. (1991). Geological Setting and Evolution of Gold Bearing Quartz Veins in the Nigerian Schist Belts. *In Proc. Symp. Brazil Gold, (E.A. Ladeira Ed.),* p. 257 – 260.

Aliyu, A., Wada, A., Ahmad, A., & Muhammad, D. (2020a). Investigation of an aerospectrometric anomaly using ground gamma ray spectrometry sheet 81, dutse north-western Nigeria. *Science Forum (Journal of Pure and Applied Sciences)*, *20*(1), 1. https://doi.org/10.5455/sf.58915

Aliyu, A., Lawal, K. M., Abubakar, I. Y., Wada, A., & Olayinka, A. L. (2020b.). Geomagnetic Studies of Pegmatite Mineralization at Lema and Ndeji North-Central, Nigeria. *Journal of Mining and Geology 56(1) 81-89.*

Ball, E. (1980). An Example of very consistent Brittle Deformation over a wide intra cratonic area: the late Pan-African Fracture System of the Toureg and Nigeiran Shields. *Tectonophysics*, 7: 363-379.

Balogun, O.B. (2019). Tectonic and structural analysis of the Migmatite–Gneiss–Quartzite complexof Ilorin area from aeromagnetic data. *NRIAG J Astron Geophysics* 8(1):22–33.

Boadi, B., Wemegah, D. D., & Preko, K. (2013). Geological and structural interpretation of the Konongo area of the Ashanti gold belt of Ghana from aero-magnetic and radiometric data. *International Research Journal of Geology and Mining (IRJGM*, *3*(3), 124–135. http://www.interesjournals.org/IRJGM

Bukola, A.S, Abbass, A.A, Adewuyia, A.R. (2021). Delineating and interpreting the gold veins within Bida and Zungeru Area, Niger State Nigeria, using aeromagnetic and radiometric data. *Pakistan J Geol (PJG)* 5(2):41–50.

Cooper, G.R.J., Cowan, D.R., 2008. Edge enhancement of potential-field data using nnormalized statistics. *Geophysics* 73 (3), H1–H4.

Dalan, R.A. (2006). A geophysical approach to buried site detection using down-hole susceptibility and soil magnetic techniques. *Archaeological Prospection* 13, pp. 182–206.

Dearing, J.A, (1994). Environmental magnetic susceptibility, using the Bartington MS2 system.

Eldosouky, A. M., Elkhateeb, S. O., Mahdy, A. M., Saad, A. A., Fnais, M. S., Abdelrahman, K., & András, P. (2022). Structural analysis and basement topography of Gabal Shilman area, South Eastern Desert of Egypt, using aeromagnetic data. *Journal of King Saud University - Science*, *34*(2). https://doi.org/10.1016/j.jksus.2021.101764

Eldosouky, A. M., Sehsah, H., Elkhateeb, S. O., & Pour, A. B. (2020). Integrating aeromagnetic data and Landsat-8 imagery for detection of post-accretionary shear zones controlling hydrothermal alterations: The Allaqi-Heiani Suture zone, South Eastern Desert, Egypt. *Advances in Space Research*, *65*(3), 1008–1024. https://doi.org/10.1016/j.asr.2019.10.030

Eldosouky, A.M., Abdelkareem, M., Elkhateeb, S.O. (2017). Integration of remote sensing andaeromagnetic data for mapping structural features and hydrothermal alteration zones in Wadi Allaqi area, South Eastern Desert of Egypt. *J. Afr. Earth Sc.* 130, 28–37.

Elkhateeb, S. O., & Abdellatif, M. A. G. (2018). Delineation potential gold mineralization zones in a part of Central Eastern Desert, Egypt using Airborne Magnetic and Radiometric data. *NRIAG Journal of Astronomy and Geophysics*, *7*(2), 361–376. https://doi.org/10.1016/j.nrjag.2018.05.010

Elkhateeb, S. O., & Abdellatif, M. A. G. (2018b). Delineation potential gold mineralization zones in a part of Central Eastern Desert, Egypt using Airborne Magnetic and Radiometric data. *NRIAG Journal of Astronomy and Geophysics*, *7*(2), 361–376. https://doi.org/10.1016/j.nrjag.2018.05.010

Evjen HM (1936) The place of the vertical gradient in gravitational interpretations. Geophysics. Society of Exploration Geophysicists 1(1): 127–136

Garba, I. (2002) Late Pan African Tectonics and Origin of Gold Mineralization and Rare-Metal Pegmatites in the Kushaka Schist Belt, Northcentral Nigeria. *Jour. Min. Geol., 38(1): 1-12*

Garba, I. (2000). Origin of Pan African Mesothermal Gold Mineralization at Bin Yauri, *Nigerian Jour. Afri. Earth Sc. 31:433-449*

Garba, I. and Akande, S.O. (1992). The Origin and Significance of Non-Aqueous CO2 Fluid Inclusions in the Auriferous Veins of Bin Yauri, Northwestern Nigeria. Mineralium Deposita, 27: 249 – 255.

Hinze, W.J. (1990). The Role of Gravity and Magnetic Methods in Engineering and Environmental Studies, In; Ward, S.H., Ed., Geotechnical and Environmental Geophysics, *Society of Exploration Geophysicists,* 1: 75 - 126.

Holden, E.J., Kovesi, P., Dentith, M., Wedge, D., Wong, J.C., Fu, S.C. (2010). Detection of regions of structural complexity within aeromagnetic data using image analysis. In: Twenty Fifth International Conference of Image and Vision Computing New Zealand.

Ibraheem IM, Haggag M, Tezkan B (2019) Edge detectors as structural imaging tools using aeromagnetic data: a case study of Sohag Area, Egypt. Geosciences. Multidisciplinary Digital Publishing Institute 9(5):211

Lawal, T. O. (2020). Integrated aeromagnetic and aeroradiometric data for delineating lithologies, structures, and hydrothermal alteration zones in part of southwestern Nigeria. *Arabian Journal of Geosciences*, *13*(16). https://doi.org/10.1007/s12517-020-05743-7

Mahdi, A. M., Eldosouky, A. M., el Khateeb, S. O., Youssef, A. M., & Saad, A. A. (2022). Integration of remote sensing and geophysical data for the extraction of hydrothermal alteration zones and lineaments; Gabal Shilman basement area, Southeastern Desert, Egypt. *Journal of African Earth Sciences*, *194*. https://doi.org/10.1016/j.jafrearsci.2022.104640

McCurry, P., 1970, *The geology of degree sheet 21 (Zaria)* [MSc thesis] Zaria, Nigeria, Ahmadu Bello University.

Okeyode, I. C., Olurin, O. T., Ganiyu, S. A., & Olowofela, J. A. (2019). High resolution airborne radiometric and magnetic studies of ilesha and its environs, southwestern Nigeria. *Materials and Geoenvironment*, *66*(1), 51–73. https://doi.org/10.2478/rmzmag-2018-0020

Ostrovskiy, E.A. (1975). Antagonism of radioactive elements in wellrock alteration fields and its use in aerogamma spectrometric prospecting. *International Geological Review,* 17: pp. 461–8.

Reid, A.B., Allsop, J. M., Granser, H., Millett, A. J., and Somerton, I.W. (1990). Magnetic interpretation in three dimensions using Euler deconvolution. *Geophysics*, **55:** 80-90.

Silva, A.M., Pires, A.C.B., McCafferty, A., Moraes, R.A.V. and Xia, H. (2003). Application of airborne geophysical data to mineral exploration in the uneven exposed terrains of the Rio Das Velhas greenstone belt. *Revista Brasileira de Geociências*, 33(2):17–28.

Tawey, M.D., Adetona, A.A., Alhassan, U.D. (2021). Aero radiometric data assessment of

hydrothermal alteration zones in parts of northcentral Nigeria. *Asian J Geol Res* 4(2):1–16.

Telford, W.M., Geldart, L.P. and Sheriff, R.E. (1990). *Applied Geophysics*, 2nd ed. Cambridge University Press.

Telford, W. M.; Geldart, L. P.; Sheriff, R. E. (2004). *Applied_Geophysics_-_Telford__Geldart__Sheriff.pdf* (p. 760).

Udensi, E.E., Osazuwa, I.B. and Daniyan, M.A. (2003). Trend Analysis of the Total Magnetic Field over the Nupe Basin, Nigeria. *Nigerian Journal of Physics*, **15** (1), ISSN 1595-0611, pp 143 - 151.

Udo, P.O. (1982). *Physical Geography of Nigeria*. Heinemann Education Publishers, Ibadan: 3-8.

Umaru AO, Danbatta UA, Muhyideen H et al (2022a) Lithological characteristics and structural analysis of basement complex rocks of Danko, Zuru Schist Belt, northwestern Nigeria: implication for structural evolution. Sci Forum (J Pure Appl Sci) 21:192–205

Umaru, A. O., Okunlola, O., Danbatta, U. A., & Olisa Olusegun, G. (2022b). Litho-structural and hydrothermal alteration mapping for delineation of gold potential zones within Kaiama, northwestern Nigeria, using airborne magnetic and radiometric data. *Arabian Journal of Geosciences*, *15*(24). https://doi.org/10.1007/s12517-022-11048-8

Woakes, M., Rahaman, M.A., Ajibade, A.A. (1987): Some Metallogenic Features of the Nigerian Basement. In Geology of Nigeria. *Journal of African Earth Science*.Vol.6 No. 5.

Wright J.B. (1976). Fracture systems in Nigeria and initiation of fracture zones in the south Atlantic, *Tectonophysics* – Elsevi.

Wemegah, D.D., Menyeh, A. and Danuor, S.K. (2009). Magnetic Susceptibility Characterization of mineralized and non mineralized rocks of the Subenso Concession of Newmont Ghana Gold Limited. In Ghana Science Association Biennial Conference, UCC.